Chemical Engineering Journal 449 (2022) 137869

Contents lists available at ScienceDirect

Chemical Engineering Journal

journal homepage: www.elsevier.com/locate/cej

Tubular catalytic polyHIPE reactor with deposited silver nanoplate nanoparticles

Rok Mravljak [a], Benjamin Božič [a], Matejka Podlogar [b], Aleš Podgornik [a,c,*]

[a] Department of Chemical Engineering and Technical Safety, Faculty of Chemistry and Chemical Technology, University of Ljubljana, Ljubljana SI-1000, Slovenia
[b] Department for Nanostructured Materials, Jožef Stefan Institute, SI-1000 Ljubljana, Slovenia
[c] COBIK, Mirce 21, 5270 Ajdovščina, Slovenia

ARTICLE INFO

Keywords:
Silver nanoplates
Microstructure
polyHIPE
Flow-through catalytic reactor
4-nitrophenol

ABSTRACT

Continuously operating heterogeneous catalytic reactors are an important step towards more efficient and controllable processes compared to batch operation. Ideally, reactors should exhibit high permeability with the catalyst having a high surface area to volume ratio to minimize the required amount. An example of such catalyst morphology are nanoparticles with a plate-like morphology. In this work, the catalytic reactor was prepared by depositing plate-like silver nanoparticles on positively charged high internal phase emulsion monoliths by exploiting their negative zeta potential. The silver nanoplates had an edge length of 63 nm and a thickness of 13 nm with a sphericity factor of 0.548. The amount of deposited silver, determined from absorbance measurement and mass difference was 12.5 mg/ml and remained unaffected by the concentration of positively charged groups in the range between 69 and 110 mmol/l, demonstrating the robustness of the proposed approach. The permeability remained unchanged after silver deposition under flow due to the polymer microstructure. The reactor was found to be stable under various elution conditions, even after prolonged catalytic reduction of 4-nitrophenol. The specific catalytic activity of silver nanoplates was 428 min^{-1} g^{-1}, which is an order of magnitude higher than that of silver nanoparticles with cuboctahedra shape and one of the highest reported. The proposed approach can be applied to various types of catalytic nanoparticles by exploiting a variety of possible interactions.

1. Introduction

High permeability of the catalyst is very important for the preparation of flow-through catalytic processes with high productivity [1]. To achieve rapid catalytic conversion, a large surface area is required, which is associated with a small size of the catalyst particles [2] and their morphology [3,4]. The combination of catalyst nanoparticles with an inert porous matrix seems to be the method of choice to prepare highly permeable catalytic reactors while minimizing the amount of required catalyst. There are several approaches to construct such catalytic reactors, either by in situ catalyst synthesis [5–12] or by depositing already pre-synthesized NP and stabilizing them by various interactions [13–15].

The matrix microstructure plays an important role in maintaining a high matrix permeability after catalyst loading. While the deposited catalyst inevitably decreases the porosity, the change in pore size should be as small as possible to avoid a substantial decrease in permeability [16]. With this in mind, high internal phase emulsion polymer (polyHIPE) monoliths seem to be a good choice. PolyHIPEs are prepared by polymerization of high internal phase emulsions, also called gel emulsions, generated by a catastrophic inversion mechanism [17]. Methacrylates are commonly used for their preparation because of their simple post modification [18]. They were implemented for different applications, among others also in catalysis [1,10,12]. Most of the polyHIPE pore surface area suitable for catalyst deposition is located within the large void pores [1,19,20], while the pressure drop has been shown to be mainly governed by the smaller interconnecting pores [21]. During in situ synthesis, silver nanoparticles (AgNP) are uniformly formed over the entire pore surface [11], including the interconnecting pores. Therefore, deposition of nanoparticles appears to be a better option, especially when loaded in a flow-through manner. In this way, the highest linear velocity within the matrix occurs in the interconnecting

* Corresponding author at: Department of Chemical Engineering and Technical Safety, Faculty of Chemistry and Chemical Technology, University of Ljubljana, Ljubljana SI-1000, Slovenia.
E-mail addresses: bb8249@student.uni-lj.si (B. Božič), ales.podgornik@fkkt.uni-lj.si (A. Podgornik).

https://doi.org/10.1016/j.cej.2022.137869
Received 22 April 2022; Received in revised form 8 June 2022; Accepted 29 June 2022
Available online 3 July 2022

pores, being much smaller than the void pores [22], so most nanoparticles pass through them and preferentially adsorb on the surface of the void pores, where the shear forces are much lower.

To design a high performance catalytic reactor, the morphology of the nanoparticles must be considered in addition to their size [23]. In this work, we focused on a catalyst based on silver metal nanocrystals, which has been extensively studied for the conversion of organic molecules [24,25], conversion of CO_2 to fuels [26,27], oxygen reduction reactions [28], redox reactions [29], and as a reducing agent in ATRP [30]. AgNPs can be prepared by various approaches in different sizes and morphologies [31–41]. As silver belongs to the Fm3m space group of the isometric cubic crystal system, when developed idiomorphically, it mostly crystallizes in the shape of a cube, octahedron, or most commonly, their combination. However, in all these morphologies the surface area to volume ratio is low and the sphericity factor ranges from 0.905 for cuboctahedron to 0.806 for cube morphology [42]. On the other hand, the combination of two octahedra or cuboctahedra in twinning, especially in contact twinning according to the spinel law, forms a triangular or hexagonal plate-like morphology [43,44] whose size and thickness can be adjusted independently by tuning the synthesis conditions [45–50]. Because of their electric conductivity, light excitation results in colorful solutions, caused by the plasmonic effect, which can be used to monitor their concentration [51–53]. The UV–Vis absorbance peak maximum of the silver nanoplates colloid enables the estimation of their size to thickness ratio [45,47,54,55]. The plasmonic effect is widely used to prepare nanoscale optical [56–58], colorimetric [59], and environmental sensors [60], for surface enhanced Raman scattering (SERS) [61], photoacoustic imaging [62], cancer diagnosis [63], light-emitting devices [64], and nanoscale hotspot generation [65,66]. Furthermore, due to high surface to volume ratio and low sphericity factor they are also promising candidate for an efficient catalyst [3]. In addition to attractive morphology, their twin planes are combined with multiple stacking faults [67], causing high reactivity of those planes, resulting in high catalytic activity [68]. In practice it is difficult to determine the catalytic activity of colored AgNP colloids in batch reactors, because their UV–Vis absorbance spectrum can overlap with that of model dyes such as 4-nitrophenol (4-NP), which are commonly converted to study the catalytic activity of metal nanoparticles, including nanoplates [69,70].

The aim of this work was to develop a platform approach for the preparation of a highly porous flow-through reactor with high catalytic activity. A functionalized polyHIPE support in combination with silver nanoplates was used as the proof of concept. Their negative zeta potential was utilized for adsorption on the polyHIPE matrix. The adsorbed amount was found to be independent on the density of positively charged groups. The catalytic activity was studied by the reduction of a common pollutant found in wastewater, namely 4-NP to non-toxic 4-aminophenol (4-AP).

2. Materials and methods

Polyvinylpyrrolidone K30 (PVP K30), boric acid (H_3BO_3), solution of 1 M silver nitrate ($AgNO_3$), 30% hydrogen peroxide H_2O_2, sodium hydroxide (NaOH), trimethylamine hydrochloride (TMAHC), tris(hydroxymethyl)aminomethane (Tris), sodium chloride (NaCl), ethanol (EtOH), and trisodium citrate (Na3cit) were purchased from Sigma-Aldrich. Sodium borohydride ($NaBH_4$) (Nokia Chemicals), 4-nitrophenol (4-NP) (Acros Organics). All chemicals were used as received without additional purification. Deionized (DI) water was filtered through a 0.2 μm filter (cellulose nitrate, Sartorius) before use.

2.1. PolyHIPE functionalization and characterization

PolyHIPE monoliths with a matrix volume of approximately 0.5 ml were prepared and characterized for permeability and open porosity as described elsewhere [11,21]. Briefly, the epoxy groups of the polyHIPE polymer were converted to quaternary amine (QA) ionizable functional groups with a basic aqueous solution of TMAHC [71]. Different molar concentrations of TMAHC, namely 0.01, 0.1, 0.15 M, were adjusted to pH 11 with NaOH. Basic conditions favor nucleophilic attack via an S_N2 mechanism on the less substituted carbon as well as the predominant formation of the free base form of TMAHC, which increases the reactivity of the nucleophile (Scheme 1). Each polyHIPE sample was immersed in 10 ml of the corresponding solution for 4 days at 8 °C. Once functionalization was complete, samples were washed extensively with DI water for several days before further characterization.

The pressure drop of the prepared polyHIPE-QA samples was measured using DI water at flow rates from 0.5 to 3 ml/min to calculate the permeability as described elsewhere [21]. Open porosity was determined by pulse injection experiments in triplets with 0.5 vol% acetone in 1 M NaCl according to the literature [21]. Briefly, the pulse response of the housing and samples was measured. The pore volume accessible to the mobile phase was calculated by subtracting the 1st moment of the empty housing from the 1st moment of the housing containing the polyHIPE-QA matrix. By dividing the calculated pore volume by the total column volume (CV), the flow-through porosity was determined.

2.2. Quantification of QA group concentration

The amount of QA groups present on the functionalized polyHIPE-QA was determined with a pH transition method as described in the literature [71]. Briefly, the measurements were performed on a high-performance liquid chromatography system (ÄKTA HPLC, Sweden) at a flow rate of 3 ml/min. The buffers used were 5 mM Tris/NaOH, pH 9.6 (buffer A) and 5 mM Tris/NaOH, 1 M NaCl, pH 9.6 (buffer B). By changing the buffers stepwise, the pH transitions were obtained and the calibration curve from the literature [71] was used to calculate the QA group concentration.

2.3. Silver nanoplates synthesis

The synthesis was prepared according to the literature with minor modifications [72]. In a wide 1 l beaker 0.78 ml of 1 M $AgNO_3$, 53 ml of 30 mM H_3BO_3 [73–75], and 53 ml of 28 g/L PVP [76–78] were diluted to 500 ml with DI water and stirred with a large Teflon magnet at 450 rpm. Then, 90 ml of a freshly prepared 10 mM $NaBH_4$ in 1.2 mM NaOH solution was slowly added to form AgNP seeds, which caused a color change to yellow and orange. The reaction was left until all bubbles formed at the top disappeared. Meanwhile, a fresh solution of 3% H_2O_2 [79–81] was prepared and slowly added after 10 min using a peristaltic pump (Masterflex, Cole-Parmer, USA) with a flow rate of 0.6 ml/min. A color change from light to dark orange, red, and finally purple was observed, indicating a change in AgNP morphology. The color change was monitored every 2 min by sampling, 11-fold dilution and measurement of UV–Vis spectra (Tecan, infinite M200Pro, Switzerland). It took about 50 min for the colloidal solution to turn purple, indicating the formation of silver nanoplates. The reaction was then continuously steered until 1.5 ml of 1 M NaOH was added to increase the pH from below 7 to 9 to stop the reaction and stabilize the colloid. The time for NaOH addition was chosen based on the following experiment: to 1 ml of the colloidal solution, 50 μl of 0.1 M NaOH was added and then the absorbance was measured. No difference in the spectra indicated the absence of Ag_2O and the completion of the reaction. The beaker was then wrapped in Al-foil and stored at room temperature until use.

2.4. Deposition of silver nanoplates on polyHIPE-QA columns

100 ml of the silver nanoplates colloidal solution with a concentration of 0.137 g/l (based on the absorption maximum) was circulated through the functionalized polyHIPE-QA monolith using the peristaltic pump at a flow rate of 1.75 ml/min. The colloidal solution was stirred

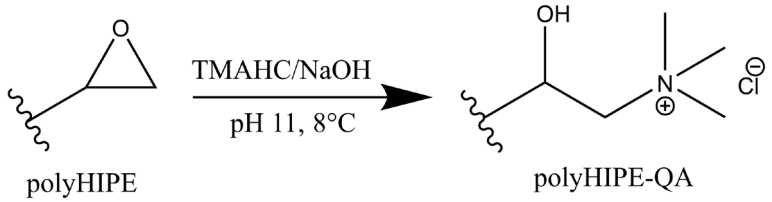

Scheme 1. Reaction scheme for the synthesis of quaternary amine functionalized polyHIPE.

during loading. Every 10 min, 50 µl samples were taken, diluted 11-fold, and UV–Vis absorbance scans were measured. The decrease in absorbance maximum allowed to monitor progress of the silver nanoplate loading. The flow was stopped once a steady state was reached. Finally, the polyHIPE-QA-AgNP monoliths were washed with DI water. Besides absorbance measurements, mass measurements (scale RC 210 D, Sartorius, Germany) of the wet monolith in triplets before and after deposition were performed to determine the quantity of catalyst deposited.

2.5. Catalytic activity for the reduction of 4-nitrophenol

The catalytic activity of the deposited silver nanoplates was determined according to the literature [11]. Briefly, a solution of 0.4 mM 4-NP, 60 mM $NaBH_4$ and 0.1 M NaOH with pH 13 to prevent $NaBH_4$ decomposition [82] and degassed to prevent oxidation of the intermediates [83]. The solution was pumped through the polyHIPE-QA-AgNP matrix at different flow rates from 2.75 to 0.75 ml/min and the absorbance at 400 nm was monitored. A polyHIPE-QA was also measured, exhibiting no catalytic activity. Open porosity of polyHIPE-QA-AgNP samples was determined (see section 2.1) and residence time was calculated by dividing it with appropriate flow rate.

2.6. Microscopy

Centrifugation (mini spin, Eppendorf, Germany) at 12,000 G for 20 min was used to induce settling of the particles. The supernatant was removed and DI water was added. The procedure was repeated 3 times. The sample holder for the scanning electron microscope (SEM) made of aluminum was previously sanded, polished and cleaned with EtOH, DI water and ultrasound for 10 s (ASonic, Slovenia). A drop of the concentrated colloidal solution was placed on a SEM holder and allowed to dry at 60 °C. The polyHIPE with deposited particles was first dried, then sanded into shape, washed with DI water, ultrasonicated for 5 s, dried in a stream of air, and mounted on a SEM holder using carbon tape (Nisshin em.co. ltd.). After drying at 60 °C, the samples were coated with a thin layer (10 nm) of carbon (PECS, model 682, Gatan). Then contacts were made with conductive silver paint (Agar scientific). Microscopy was performed with FEG-SEM (Verios 4G HP, Thermo Fischer Scientific, USA) and FE-SEM (Zeiss ULTRA plus, ZEISS, Oberkochen, Germany).

3. Results and discussion

To introduce positive charges on the polyHIPE matrix, appropriate chemical groups must be present after polymerization to allow functionalization. While plethora of different chemistries have already been used for their preparation [84], methacrylate polyHIPEs seem to be especially suitable due to the presence of epoxy groups that are easily converted into other functionalities [85]. Strong ion-exchange groups were chosen in this study, because they exhibit a constant charge over a wide pH range, thus ensuring system robustness. Positively charged quaternary amine (QA) groups were selected, due to a negative zeta potential of silver nanoparticles around neutral pH and above [86]. Although the modification procedures for the conversion of epoxide groups into QA groups are already well established [71], the precise determination of their amount in a noninvasive manner was introduced rather recently [71,87,88]. The determination is based on the pH transition using two mobile phases with the same pH but different ionic strength [87,89]. When the groups present on a matrix have an ionizable character, they are titrated during the stepwise buffer exchange and cause a pH shift. It was demonstrated that the duration and height of the pH transition shift is linearly proportional to the amount of ionizable groups [71,88].

To investigate whether the amount of loaded silver catalyst depends on the concentration of QA groups, polyHIPE-QA samples with three different QA concentrations were prepared and evaluated by the pH transition method, as shown in Fig. 1.

Fig. 1 shows that pH transitions of different heights were obtained for different polyHIPE-QA samples. Using the calibration curve developed recently for the same matrix type [71], the amount of QA groups was estimated to be 69, 101, and 110 mmol/l. The high group density indicates the possibility of strong silver nanoplate adsorption [86]. Before loading with silver nanoplates, polyHIPE-QA samples were extensively washed with DI water and weighed. Their permeability, determined by pressure drop measurements at different flow rates, was 3×10^{-14} m^2. The open accessible porosity, determined by the pulse response using NaCl and acetone as the tracer, was around 80%.

Silver nanoplates were prepared by a slow addition of H_2O_2 as described in Materials and method section. This approach allowed the preparation of silver nanoplates of the desired size and morphology by monitoring the UV–Vis absorbance of the colloid at different volumes of added H_2O_2. Over 3 l of silver nanoplates with a concentration of 0.137 g/l were prepared. Their absorbance spectrum with added light spectrum, the calibration curve and the SEM image together with the estimated particle length and thickness with fitted Gaussian distribution

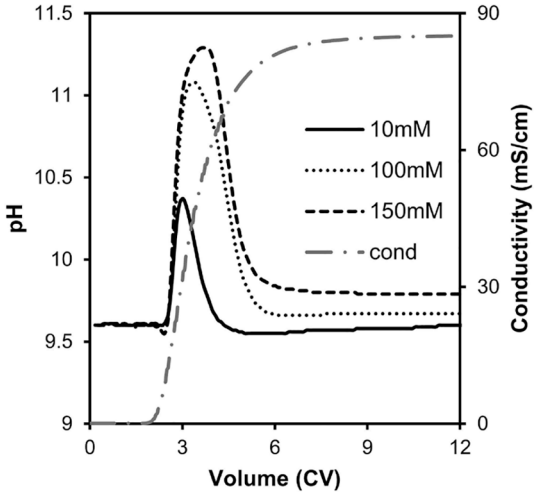

Fig. 1. The pH transition profiles with corresponding conductivity for polyHIPE bearing positively charged QA groups prepared with different concentrations of TMAHC/NaOH reagent. Experiments were performed on a high-performance liquid chromatography system ÄKTA at a flow rate of 3 ml/min. The buffers used were 5 mM Tris/NaOH, pH 9.6 (buffer A) and 5 mM Tris/NaOH, 1 M NaCl, pH 9.6 (buffer B).

are shown in Fig. 2.

The absorbance spectrum shows a maximum at 559 nm (Fig. 2a), demonstrating a pronounced plasmonic effect [51]. The SEM image shows that the average nanoplate size was approximately 63 nm with a thickness of 13 nm, which is consistent with the measured absorbance peak [45,47,54]. The synthesized silver nanoplates have both triangular and hexagonal shapes in approximately the same ratio, resulting in an average sphericity factor of only 0.548. Therefore, they have a much higher surface area to volume ratio than other morphologies typical for AgNPs. For this reason, a higher specific catalytic activity is expected.

Because of the high absorbance of the silver nanoplate colloid, we were able to monitor the loading process simply by measuring the decrease in absorbance. The calibration curve shown in Fig. 2b, measured at 559 nm for different nanoplate concentrations, showed a linear trend within a wide range of dilutions, allowing accurate on-line monitoring of the amount of loaded silver nanoplates. By centrifuging the colloid, drying and weighing, a direct correlation between absorbance and mass concentration of silver nanoplates was established.

Since the average size of the polyHIPE interconnecting pores is 1.3 μm [21], while the average size of the silver nanoplates is only 63 nm, they should be easily deposited on the matrix surface without pore clogging, thus ensuring uniform surface coverage. Typical absorbance profiles measured during loading are shown in Fig. 3. The rapid initial decrease in absorbance indicates strong adsorption of silver nanoplates to the polyHIPE-QA monoliths, suggesting that this approach might result in the formation of a stable silver-based catalytic reactor.

The same deposition procedure was repeated for all polyHIPE-QA monoliths with a different charge density. A good match was obtained for the loaded silver nanoplate mass estimated from the measured difference in UV–Vis absorbance and weight difference before and after loading. The results for polyHIPE-QA saturated with silver nanoplates as a function of QA group concentration are shown in Fig. 4a showing that the mass of deposited silver nanoplates is independent of the QA group density. This indicates extremely strong binding, which has been reported for the adsorption of biological NP such as viruses [90]. This finding is important since it shows that even substantial variations in QA group density do not affect the amount of deposited silver nanoplates.

After loading was completed, samples were washed extensively with DI water to remove unbound silver nanoplates still present in the polyHIPE-QA-AgNP pores. The permeability of the samples was then measured again and found to be unchanged for all samples. This indicates that very few, if any, silver nanoplates were adsorbed on the interconnecting pores, conclusion supported also by SEM images (Fig. 4b). Nevertheless, some decrease in permeability after loading is to be expected, since the deposition of silver nanoplates inevitably leads to a decrease in the total open porosity. The change in porosity can be estimated from the loaded silver mass. As shown in Fig. 4a, the average mass of loaded silver nanoplates was about 12.5 mg/ml. At a silver density of 10.5 g/ml [91], the loaded volume of silver occupying the pore volume is 0.6 μl. When the open porosity of polyHIPE is 0.8, the reduction in porosity by the introduced AgNP is only 0.15%. Because the permeability of polyHIPE monoliths is proportional to the porosity [21], the permeability is expected to decrease by the same percentage, which is too small to be detected experimentally.

To verify the practicality of the prepared catalytic reactors, we decided to also investigate their stability. This was done by pumping a solution of 1 M Na3cit at pH 13 through the reactor. Citrate is known to bind to the octahedral {1 1 1} crystal faces of silver [74], therefore it might act as a displacer and desorb AgNP from the pore surface, a phenomenon that has been described in chromatography of large

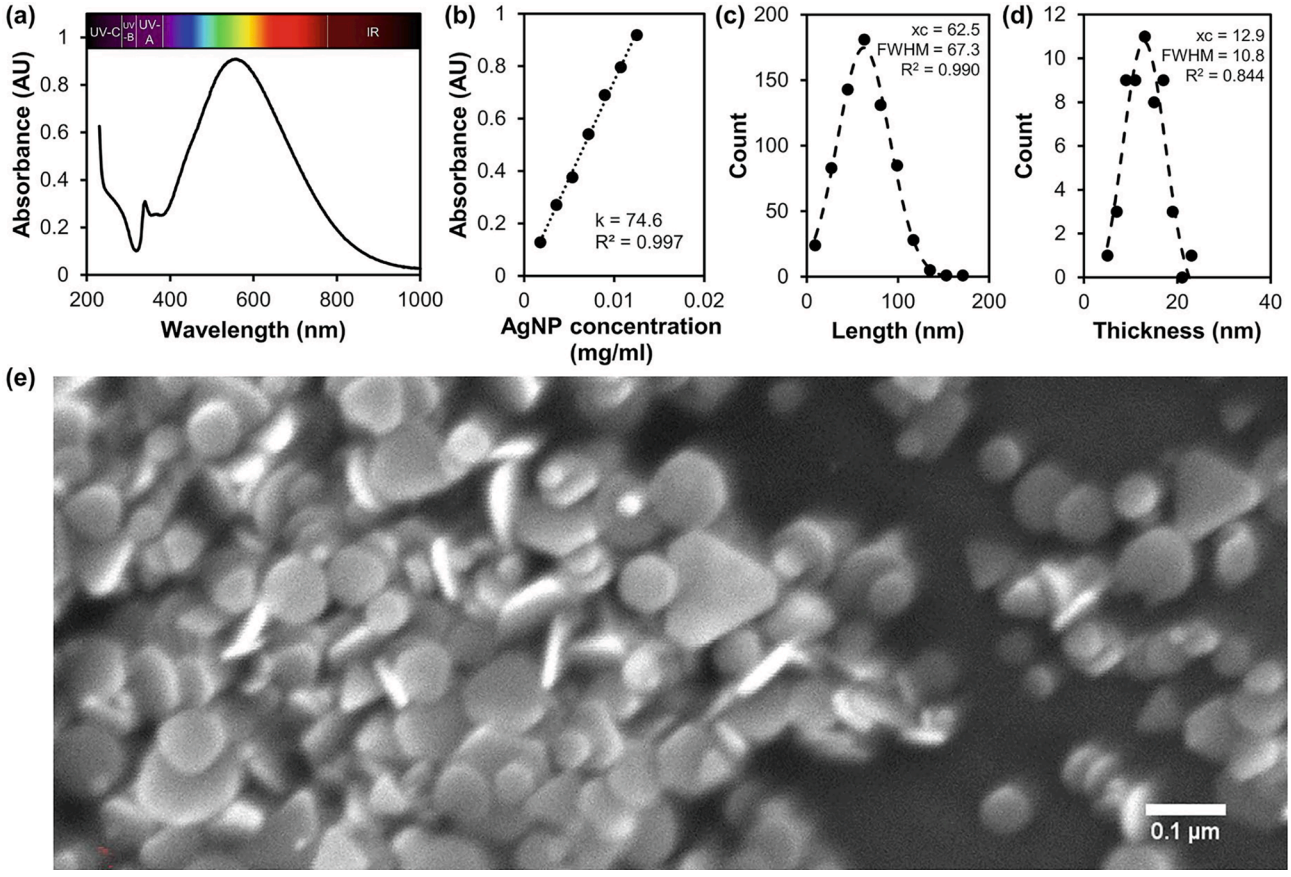

Fig. 2. (a) UV–Vis absorbance spectrum of 11-times diluted colloidal solution of silver nanoplate exhibiting peak maximum at 559 nm with light spectrum inset; (b) corresponding calibration curve at 559 nm; (e) SEM image showing spinel law twinned silver nanoplates with triangular and hexagonal morphology; (c) nanoplate edge length and (d) thickness counts with fitted Gaussian distribution estimated from SEM images.

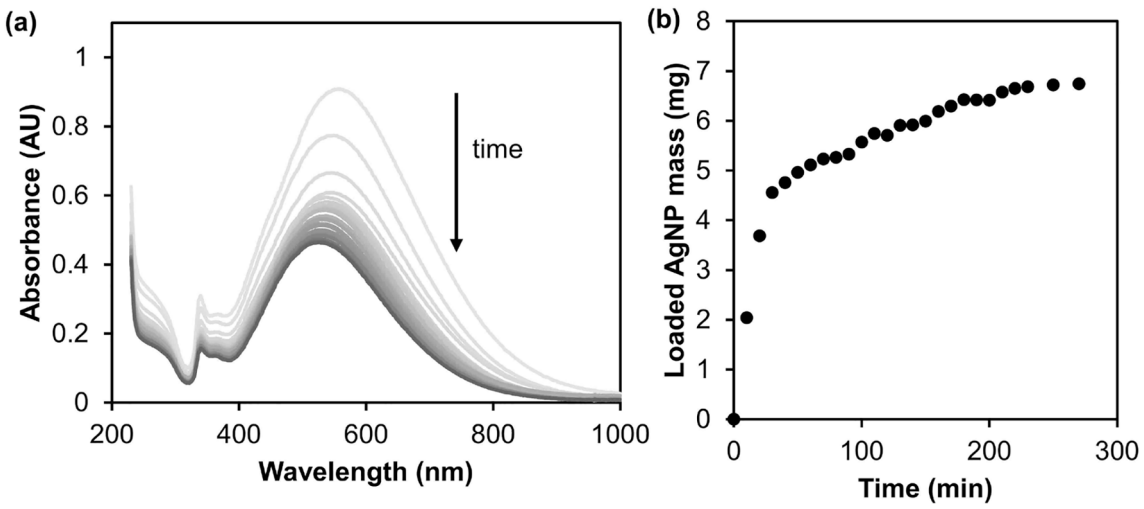

Fig. 3. (a) Loading progress of purple colloid of silver nanoplates onto positively charged polyHIPE columns showing a decrease in the UV–Vis absorbance spectrum maximum. Samples were regularly taken and absorbance was measured off-line. (b) calculated mass of deposited silver nanoplates loaded onto positively charged polyHIPE-QA versus deposition time estimated from absorbance maximum and calibration curve (Fig. 2b).

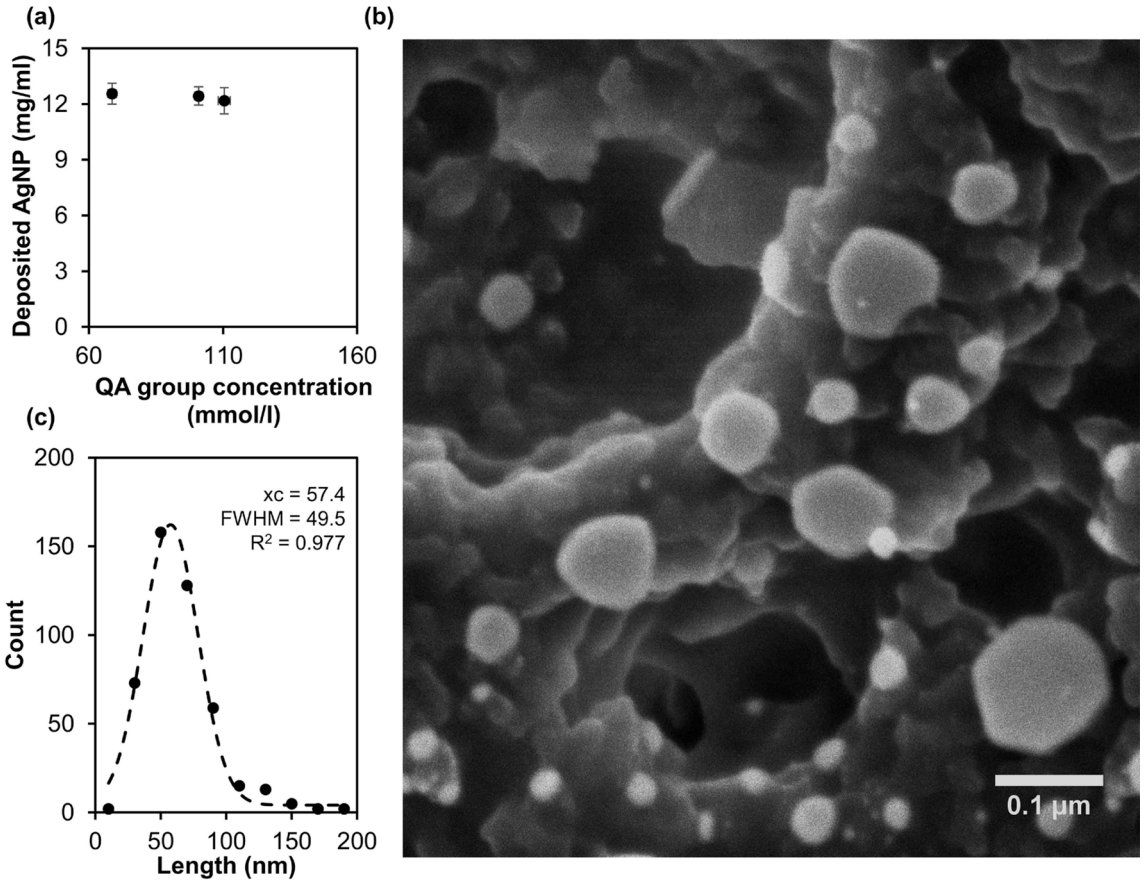

Fig. 4. (a) Maximum amount of loaded silver nanoplates as a function of positively charged QA group density in mmol of QA groups per liter of polyHIPE estimated from absorbance difference after polyHIPE saturation, (b) representative SEM image of polyHIPE with loaded nanoplates, and (c) particle edge length count estimated from SEM images with fitted Gaussian distribution.

macromolecules [92]. Moreover, at pH 13, even strong positively charged QA groups interactions are weakened [93], possibly facilitating desorption. To verify if AgNP desorption occurs, the silver reactor was washed by 20 ml of Na3cit solution (equivalent to 40 sample volumes) at the flow rate of 1 ml/min and the outlet absorbance at 559 nm was monitored. No changes were observed (data not shown). Furthermore, the reactor was immersed in the same solution and left for 3 days at room temperature. Again, there was no change in the absorbance at 559 nm. From these results it was concluded that prepared catalytic reactors are stable and can be tested for catalytic activity.

Catalytic activity was tested using an extensively studied model reaction of the reduction of 4-NP to 4-aminophenol according to the

procedure described in details elsewhere [11]. The difference between the on-line absorbance of the solution measured at 400 nm at the reactor outlet and inlet allowed estimation of the 4-NP conversion. The flow rate of the reagent through the catalytic reactor, which defines the residence time for the reaction, changed, affecting the estimated conversion, as shown in Fig. 5a and 5b. Since $NaBH_4$ was in high excess, pseudo-first-order reaction kinetics was assumed [11], which fitted well experimental data (Fig. 5b). From the fitting kinetics equation (conversion $= e^{-kt}$), considering the amount of loaded AgNP catalyst, the apparent catalytic rate constant (k_{cat}'), shown in Fig. 5c, was calculated for all samples.

It can be seen that the specific catalytic activity was independent of the deposited AgNP mass, showing that the different QA group concentration had no influence and that the proposed approach is robust. When comparing the values determined for a catalytic reactor with cuboctahedra morphology prepared by on-matrix synthesis using Tollens reagent [11], an order of magnitude higher catalytic activity was observed. This demonstrates the superiority of silver nanoplates in their catalytic activity, which was expected due to their low sphericity factor. However, the such large difference must also be attributed to higher reactivity, probably caused by the reactive twinned planes and stacking faults [36,68,94]. Comparison with some literature results where the same reaction for AgNP catalytic activity was investigated shows that the obtained value is one of the highest reported (Table 1). Significantly higher value was found only for 1-dimensional nanobelts determined in batch mode [99], while their application in a flow through might be challenging. Our results therefore indicate high potential of the proposed approach.

Finally, long-term stability was tested by successive catalytic experiments over a period of one week. No change in activity was observed (data not shown), again confirming that despite the harsher conditions in the mobile phase, there was no washout of the silver nanoplates due to the application of the reagents, neither a decrease in their catalytic activity. This shows that the presented approach allows the preparation of a robust and stable catalytic reactors.

Since the reaction rate for the tested catalytic reaction, can be approximated with a first order kinetics, the catalytic reactor productivity (Pr) can be described as follows [11]:

$$Pr = C_{in}\left(1 - e^{-k_{cat}' m_{cat}\frac{V_c\varepsilon}{F}}\right)\frac{F}{V_c}$$

where C_{in} is the inlet 4-NP concentration (g/ml), k_{cat}' catalytic rate constant (min^{-1} g^{-1}), m_{cat} AgNP mass (g), F flow rate through the reactor (ml/min), V_c reactor volume (ml), and ε the open porosity (/).

For high flow rates, productivity rapidly approaches a plateau [11], which can be determined by taking the limit of the flow rate approaching infinity:

$$Pr_{max} = \lim_{F\to\infty}\left(C_{in}\left[1 - e^{-k_{cat}' m_{cat}\frac{V_c\varepsilon}{F}}\right]\frac{F}{V_c}\right) = C_{in}k_{cat}' m_{cat}\varepsilon$$

The expression for the limit shows that, as expected, the maximum productivity (Pr_{max}) depends on the concentration of the inlet reagent, catalytic activity constant, catalyst mass, and interestingly, also on the porosity. This is an important conclusion since a typical value of porosity for particulate catalysts matrix is only about 0.36 [100], and even for most monolithic supports values of about 0.6–0.7 are reported [101]. Since polyHIPE monoliths retain mechanical stability even at a porosity of at least 0.9 [21], such porosity is already in the range of metallic foams, which however have much larger pores and thus a much lower specific surface area [102]. For this reason, polyHIPE monoliths seem to be an excellent support for the fabrication of tubular catalytic reactors with high permeability and productivity.

Although the practical verification of the proposed principle was performed only on silver nanoplates, one can imagine that it can be easily extended to other catalysts of interest that exhibit such morphology and negative zeta potential, such as platinum [103], iridium [104], copper [105], gold [106,107], palladium [108], and rhodium [109]. Moreover, due to the versatility of polyHIPE surface modification and group density control [71], targeted interactions can be introduced to allow adsorption of other materials of interest, such as metal oxides which can be prepared with similar morphologies, like magnetite (Fe_3O_4) [110,111] and Al_2O_3 [112], but also other hierarchical structures with low sphericity factor and therefore high surface area to volume ratio, such as multilevel branched TiO_2 nanocrystals [113]. As demonstrated, the presented flow-through reactor maintains high permeability after catalyst loading and is therefore ideal for studying intrinsic catalyst properties even at high flow rates since there are no diffusion limitations. Furthermore, the amount of loaded catalyst can be precisely measured, the specific activity can be accurately determined, allowing for catalyst characterization and further optimization.

4. Conclusion

A simple method for the preparation of highly efficient catalytic reactors based on silver nanoplates was studied for the first time. The nanoparticles were pumped through the quaternary amine functionalized polyHIPE matrix up to a total concentration of 12.5 mg/ml. The nanoplates with size of 63 nm provided catalytic activity that was one of the highest reported in literature reaching 428 min^{-1} g^{-1}. Due to the peculiar matrix microstructure, no measurable change in permeability after silver nanoplates loading in a flow occurred, allowing simple

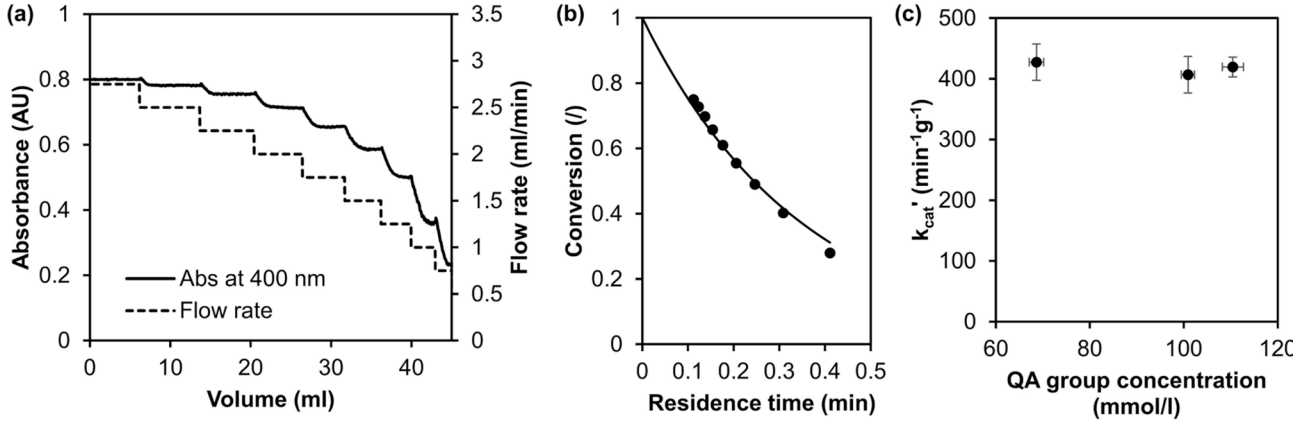

Fig. 5. (a) Change in absorbance of 4-NP at 400 nm as a function of flow rate measured at outlet of polyHIPE-QA-AgNP catalytic reactor with 69 mmol/l QA groups; (b) 4-NP conversion fitted with first-order reaction kinetics as a function of residence time; (c) the average apparent catalytic constants for the polyHIPE-QA-AgNP catalytic reactors with different concentrations of QA groups.

Table 1
Survey of the reactant concentrations, mass of AgNP catalyst and apparent catalytic rate constants for the catalytic reduction of 4-NP to 4-AP with $NaBH_4$. Table abbreviations: polyaniline (PANI), microporous organic polymer sponge (MOBS), polypyrrole (PPy), polystyrene-methyl acrylic acid (PSMAA), and multi walled carbon nanotubes (MWCNT), silver nanobelts (AgNB).

Catalyst	[4-NP] (mM)	[$NaBH_4$] (mM)	m(AgNP) (mg)	pH	Degas or N_2	k' (min^{-1})	k_{cat}' (min^{-1} g^{-1})	Ref.
Ag.nanoplate /polyHIPE	0.4	60	12.5	Yes	Yes	5.35	428	This study
AgNP /polyHIPE	0.4	60	12 – 477	Yes	Yes	0.447 – 9.03	37.3 – 18.9	[11]
Ag/PANI	0.16	16	0.005	No	No	0.056	11.2	[95]
Ag/MOBS	0.1	40	3.2	No	No	0.457	0.14	[8]
Ag/PPy	0.079	33	0.0025	No	No	0.011	4.4	[96]
Ag/PSMAA	0.074	11	2	No	No	0.492	0.25	[97]
Ag/MWCNT	0.05	2.5	0.025	No	No	0.473	18.9	[98]
AgNB	0.1	10	0.2	No	No	1.04	5220	[99]

design of the catalytic process, operating at high flow rates without pressure drop challenges. Despite non-covalent interactions between the polymer and silver catalyst, no elution was observed under any of the tested conditions, demonstrating the long-term stability and robustness of the prepared catalytic reactors. Since the surface properties of the polyHIPE pores can be adjusted, this support provides a universal matrix for the facile preparation of robust, highly permeable catalytic reactors with targeted selectivity that operate efficiently in a continuous flow-through process. This is further facilitated by flexibility of tailoring independently size of pore voids and interconnecting pores, adjusting therefore matrix to particular nanoparticle size.

Declaration of Competing Interest

The authors declare that they have no known competing financial interests or personal relationships that could have appeared to influence the work reported in this paper.

Data availability

No data was used for the research described in the article.

Acknowledgment

The financial support is gratefully acknowledged from the Slovenian Research Agency (ARRS) through project J2-9440 and program P1-0153. We want to thank Ožbej Bizjak and Samo Stankovič for technical assistance.

References

[1] K.M.L. Taylor-Pashow, J.G. Pribyl, PolyHIPEs for Separations and Chemical Transformations: A Review, Solvent Extr. Ion Exch. 37 (2019) 1–26, https://doi.org/10.1080/07366299.2019.1592924.
[2] J.A. Johnson, J.J. Makis, K.A. Marvin, S.E. Rodenbusch, K.J. Stevenson, Size-Dependent Hydrogenation of p-Nitrophenol with Pd Nanoparticles Synthesized with Poly(amido)amine Dendrimer Templates, J. Phys. Chem. C. 117 (2013) 22644–22651, https://doi.org/10.1021/jp4041474.
[3] V. Bansal, V. Li, A.P. O'Mullane, S.K. Bhargava, Shape dependent electrocatalytic behaviour of silver nanoparticles, CrystEngComm. 12 (2010) 4280–4286, https://doi.org/10.1039/c0ce00215a.
[4] M. Trojanowicz, Flow Chemistry in Contemporary Chemical Sciences: A Real Variety of Its Applications, Molecules. 25 (2020) 1434, https://doi.org/10.3390/molecules25061434.
[5] W.-M. Cheng, C.-C. Wang, C.-Y. Chen, The influence of Ni nanoparticles and Ni (II) on the growth of Ag dendrites immobilized on the chelating copolymer membrane, Mater. Chem. Phys. 137 (2012) 76–84, https://doi.org/10.1016/j.matchemphys.2012.08.029.
[6] Y.-K. Kim, D.-H. Min, Surface confined successive growth of silver nanoplates on a solid substrate with tunable surface plasmon resonance, RSC Adv. 4 (2014) 6950, https://doi.org/10.1039/c3ra44280b.
[7] J. Song, J. Hou, L. Tian, Y. Guan, Y. Zhang, X.X. Zhu, Growth of giant silver dendrites on layer-by-layer assembled films, Polymer (Guildf). 63 (2015) 237–243, https://doi.org/10.1016/j.polymer.2015.03.009.
[8] J.G. Kim, M.C. Cha, J. Lee, T. Choi, J.Y. Chang, Preparation of a Sulfur-Functionalized Microporous Polymer Sponge and In Situ Growth of Silver Nanoparticles: A Compressible Monolithic Catalyst, ACS Appl. Mater. Interfaces. 9 (2017) 38081–38088, https://doi.org/10.1021/acsami.7b14807.
[9] W. Yuan, X. Chen, Y. Xu, C. Yan, Y. Liu, W. Lian, Y. Zhou, Z. Li, Preparation and recyclable catalysis performance of functional macroporous polyHIPE immobilized with gold nanoparticles on its surface, RSC Adv. 8 (2018) 5912–5919, https://doi.org/10.1039/C8RA00089A.
[10] L. Tan, B. Tan, Functionalized hierarchical porous polymeric monoliths as versatile platforms to support uniform and ultrafine metal nanoparticles for heterogeneous catalysis, Chem. Eng. J. 390 (2020), 124485, https://doi.org/10.1016/j.cej.2020.124485.
[11] R. Mravljak, O. Bizjak, B. Božič, M. Podlogar, A. Podgornik, Flow-Through PolyHIPE Silver-Based Catalytic Reactor, Polymers (Basel). 13 (2021) 880, https://doi.org/10.3390/polym13060880.
[12] Y. Wan, Y. Feng, D. Wan, M. Jin, Polyamino amphiphile mediated support of platinum nanoparticles on polyHIPE as an over 1500-time recyclable catalyst, RSC Adv. 6 (2016) 109253–109258, https://doi.org/10.1039/C6RA19013H.
[13] G. Akay, B. Calkan, Preparation of Nanostructured Microporous Metal Foams through Flow Induced Electroless Deposition, J. Nanomater. 2015 (2015) 1–17, https://doi.org/10.1155/2015/275705.
[14] U. Černigoj, J. Gašperšič, A. Fichtenbaum, N. Lendero Krajnc, J. Vidič, G. Mitulović, A. Štrancar, Titanium dioxide nanoparticle coating of polymethacrylate-based chromatographic monoliths for phosphopetides enrichment, Anal. Chim. Acta. 942 (2016) 146–154, https://doi.org/10.1016/j.aca.2016.08.044.
[15] Z. Yang, T.-A. Asoh, H. Uyama, A cellulose monolith supported metal/organic framework as a hierarchical porous material for a flow reaction, Chem. Commun. 56 (2020) 411–414, https://doi.org/10.1039/C9CC08232H.
[16] A. Podgornik, Pressure drop in liquid chromatography, J. Sep. Sci. 42 (2019) 72–88, https://doi.org/10.1002/jssc.201800882.
[17] Y. Liu, Phase Inversion: A Superior Way to Make Emulsions, in: Encycl. Surf. Colloid Sci. Third Ed., Taylor & Francis, 2015: pp. 5362–5375. 10.1081/E-ESCS3-120049478.
[18] J. Majer, P. Krajnc, Amine Functionalisations of Glycidyl methacrylate Based PolyHIPE Monoliths, Macromol. Symp. 296 (2010) 5–10, https://doi.org/10.1002/masy.201051002.
[19] I. Pulko, P. Krajnc, High internal phase emulsion templating - A path to hierarchically porous functional polymers, Macromol. Rapid Commun. 33 (2012) 1731–1746, https://doi.org/10.1002/marc.201200393.
[20] S. Jerenec, M. Šimić, A. Savnik, A. Podgornik, M. Kolar, M. Turnšek, P. Krajnc, Glycidyl methacrylate and ethylhexyl acrylate based polyHIPE monoliths: Morphological, mechanical and chromatographic properties, React. Funct. Polym. 78 (2014) 32–37, https://doi.org/10.1016/j.reactfunctpolym.2014.02.011.
[21] R. Mravljak, O. Bizjak, M. Podlogar, A. Podgornik, Effect of polyHIPE porosity on its hydrodynamic properties, Polym. Test. 93 (2021), 106590, https://doi.org/10.1016/j.polymertesting.2020.106590.
[22] P. Hainey, I.M. Huxham, B. Rowatt, D.C. Sherrington, L. Tetley, Synthesis and ultrastructural studies of styrene-divinylbenzene Polyhipe polymers, Macromolecules. 24 (1991) 117–121, https://doi.org/10.1021/ma00001a019.
[23] Y. Xia, Y. Xiong, B. Lim, S.E. Skrabalak, Shape-controlled synthesis of metal nanocrystals: Simple chemistry meets complex physics? Angew. Chemie - Int. Ed. 48 (2009) 60–103, https://doi.org/10.1002/anie.200802248.
[24] L. Shaker Ardakani, A. Surendar, L. Thangavelu, T. Mandal, Silver nanoparticles (Ag NPs) as catalyst in chemical reactions, Synth. Commun. 51 (2021) 1–21, https://doi.org/10.1080/00397911.2021.1894450.
[25] A. Ohtaka, Recent Progress of Metal Nanoparticle Catalysts for C-C Bond Forming Reactions, Catalysts. 11 (2021) 1266, https://doi.org/10.3390/catal11111266.
[26] Y. Yoon, A.S. Hall, Y. Surendranath, Tuning of Silver Catalyst Mesostructure Promotes Selective Carbon Dioxide Conversion into Fuels, Angew. Chemie Int. Ed. 55 (2016) 15282–15286, https://doi.org/10.1002/anie.201607942.
[27] S. Suter, S. Haussener, Optimizing mesostructured silver catalysts for selective carbon dioxide conversion into fuels, Energy Environ. Sci. 12 (2019) 1668–1678, https://doi.org/10.1039/c9ee00656g.

[28] C.C.M. Neumann, E. Laborda, K. Tschulik, K.R. Ward, R.G. Compton, Performance of silver nanoparticles in the catalysis of the oxygen reduction reaction in neutral media: Efficiency limitation due to hydrogen peroxide escape, Nano Res. 6 (2013) 511–524, https://doi.org/10.1007/s12274-013-0328-4.
[29] K. Mallick, M. Witcomb, M. Scurrell, Silver nanoparticle catalysed redox reaction: An electron relay effect, Mater. Chem. Phys. 97 (2006) 283–287, https://doi.org/10.1016/j.matchemphys.2005.08.011.
[30] V.A. Williams, T.G. Ribelli, P. Chmielarz, S. Park, K. Matyjaszewski, A silver bullet: Elemental silver as an efficient reducing agent for atom transfer radical polymerization of acrylates, J. Am. Chem. Soc. 137 (2015) 1428–1431, https://doi.org/10.1021/ja512519j.
[31] D. Yu, V.-W.-W. Yam, Controlled Synthesis of Monodisperse Silver Nanocubes in Water, J. Am. Chem. Soc. 126 (2004) 13200–13201, https://doi.org/10.1021/ja046037r.
[32] B. Wiley, Y. Sun, Y. Xia, Synthesis of silver nanostructures with controlled shapes and properties, Acc. Chem. Res. 40 (2007) 1067–1076, https://doi.org/10.1021/ar7000974.
[33] M.F.H. Abd El-Kader, M.T. Elabbasy, M.K. Ahmed, A.A. Menazea, Structural, morphological features, and antibacterial behavior of PVA/PVP polymeric blends doped with silver nanoparticles via pulsed laser ablation, J. Mater. Res. Technol. 13 (2021) 291–300, https://doi.org/10.1016/j.jmrt.2021.04.055.
[34] A. Jakab, C. Rosman, Y. Khalavka, J. Becker, A. Trügler, U. Hohenester, C. Sönnichsen, Highly sensitive plasmonic silver nanorods, ACS Nano. 5 (2011) 6880–6885, https://doi.org/10.1021/nn200877b.
[35] B. Bari, J. Lee, T. Jang, P. Won, S.H. Ko, K. Alamgir, M. Arshad, L.J. Guo, Simple hydrothermal synthesis of very-long and thin silver nanowires and their application in high quality transparent electrodes, J. Mater. Chem. A. 4 (2016) 11365–11371, https://doi.org/10.1039/c6ta03308c.
[36] C. Wang, Z. Zhang, G. Yang, Q. Chen, Y. Yin, M. Jin, Creation of Controllable High-Density Defects in Silver Nanowires for Enhanced Catalytic Property, Nano Lett. 16 (2016) 5669–5674, https://doi.org/10.1021/acs.nanolett.6b02317.
[37] M. Parente, M. Van Helvert, R.F. Hamans, R. Verbroekken, R. Sinha, A. Bieberle-Hütter, A. Baldi, Simple and Fast High-Yield Synthesis of Silver Nanowires, Nano Lett. 20 (2020) 5759–5764, https://doi.org/10.1021/acs.nanolett.0c01565.
[38] Y. Gao, B. Pinho, L. Torrente-Murciano, Tailoring the size of silver nanoparticles by controlling mixing in microreactors, Chem. Eng. J. 432 (2022), 134112, https://doi.org/10.1016/j.cej.2021.134112.
[39] K. Nathanael, P. Pico, N.M. Kovalchuk, A.D. Lavino, M.J.H. Simmons, O.K. Matar, Computational modelling and microfluidics as emerging approaches to synthesis of silver nanoparticles – A review, Chem. Eng. J. 436 (2022), 135178, https://doi.org/10.1016/j.cej.2022.135178.
[40] A.A. Menazea, H.M. Assaggaf, S. Alghamdi, E.H. Eldrehmy, M.T. Elabbasy, M.F. H. Abd El-Kader, Fundamentals, antibacterial, and photocatalysis properties of Ag@Se@PVDF nanocomposite membrane synthesized via laser ablation technique, J. Mater. Sci. Mater. Electron. 33 (2022) 1021–1029, https://doi.org/10.1007/s10854-021-07372-6.
[41] M. El-Sharnouby, A. El Askary, N.S. Awwad, H.A. Ibrahium, M.E. Moustapha, M. O. Farea, A.A. Menazea, A.M. Abdelghany, Enhanced Electrical Conductivity and Dielectric Performance of Ternary Nanocomposite Film of PEMA/PS/Silver NPs Synthesized by Laser Ablation, J. Inorg. Organomet. Polym. Mater. (2022) 1–10, https://doi.org/10.1007/s10904-022-02286-0.
[42] H. Wadell, Volume, Shape, and Roundness of Quartz Particles, J. Geol. 43 (1935) 250–280, https://doi.org/10.1086/624298.
[43] C. Lofton, W. Sigmund, Mechanisms Controlling Crystal Habits of Gold and Silver Colloids, Adv. Funct. Mater. 15 (2005) 1197–1208, https://doi.org/10.1002/adfm.200400091.
[44] J.E. Millstone, S.J. Hurst, G.S. Métraux, J.I. Cutler, C.A. Mirkin, Colloidal gold and silver triangular nanoprisms, Small. 5 (2009) 646–664, https://doi.org/10.1002/smll.200801480.
[45] D. Aherne, D.M. Ledwith, M. Gara, J.M. Kelly, Optical Properties and Growth Aspects of Silver Nanoprisms Produced by a Highly Reproducible and Rapid Synthesis at Room Temperature, Adv. Funct. Mater. 18 (2008) 2005–2016, https://doi.org/10.1002/adfm.200800233.
[46] T. Huang, X.-H.-N. Xu, Synthesis and characterization of tunable rainbow colored colloidal silver nanoparticles using single-nanoparticle plasmonic microscopy and spectroscopy, J. Mater. Chem. 20 (2010) 9867, https://doi.org/10.1039/c0jm01990a.
[47] J.M. Kelly, G. Keegan, M.E. Brennan-Fournetb, Triangular silver nanoparticles: Their preparation, functionalisation and properties, Acta Phys. Pol. A. 122 (2012) 337–345. 10.12693/APhysPolA.122.337.
[48] B. Tang, S. Xu, X. Hou, J. Li, L. Sun, W. Xu, X. Wang, Shape Evolution of Silver Nanoplates through Heating and Photoinduction, ACS Appl. Mater. Interfaces. 5 (2013) 646–653, https://doi.org/10.1021/am302072u.
[49] Q. Zhang, Y. Yang, J. Li, R. Iurilli, S. Xie, D. Qin, Citrate-free synthesis of silver nanoplates and the mechanistic study, ACS Appl. Mater. Interfaces. 5 (2013) 6333–6345, https://doi.org/10.1021/am401374x.
[50] Y.N. Wijaya, J. Kim, W.M. Choi, S.H. Park, M.H. Kim, A systematic study of triangular silver nanoplates: One-pot green synthesis, chemical stability, and sensing application, Nanoscale. 9 (2017) 11705–11712, https://doi.org/10.1039/c7nr03077k.
[51] N.E. Motl, A.F. Smith, C.J. Desantis, S.E. Skrabalak, Engineering plasmonic metal colloids through composition and structural design, Chem. Soc. Rev. 43 (2014) 3823–3834, https://doi.org/10.1039/c3cs60347d.
[52] J. Zhao, A.O. Pinchuk, J.M. McMahon, S. Li, L.K. Ausman, A.L. Atkinson, G. C. Schatz, Methods for describing the electromagnetic properties of silver and gold nanoparticles, Acc. Chem. Res. 41 (2008) 1710–1720, https://doi.org/10.1021/ar800028j.
[53] J. Zheng, Y. Ding, B. Tian, L.W. Zhong, X. Zhuang, Luminescent and raman active silver nanoparticles with polycrystalline structure, J. Am. Chem. Soc. 130 (2008) 10472–10473, https://doi.org/10.1021/ja803302p.
[54] R. Jin, Y. Charles Cao, E. Hao, G.S. Métraux, G.C. Schatz, C.A. Mirkin, Controlling anisotropic nanoparticle growth through plasmon excitation, Nature. 425 (2003) 487–490, https://doi.org/10.1038/nature02020.
[55] D.E. Charles, D. Aherne, M. Gara, D.M. Ledwith, Y.K. Gun'ko, J.M. Kelly, W. J. Blau, M.E. Brennan-Fournet, Versatile Solution Phase Triangular Silver Nanoplates for Highly Sensitive Plasmon Resonance Sensing, ACS Nano. 4 (1) (2010) 55–64.
[56] A.J. Haes, L. Chang, W.L. Klein, R.P. Van Duyne, Detection of a Biomarker for Alzheimer's Disease from Synthetic and Clinical Samples Using a Nanoscale Optical Biosensor, J. Am. Chem. Soc. 127 (2005) 2264–2271, https://doi.org/10.1021/ja044087q.
[57] J.N. Anker, W.P. Hall, O. Lyandres, N.C. Shah, J. Zhao, R.P. Van, Duyne, Biosensing with plasmonic nanosensors, in: Nanosci. Technol, Co-Published with Macmillan Publishers Ltd, UK, 2009, pp. 308–319, https://doi.org/10.1142/9789814287005_0032.
[58] G. Bodelón, V. Montes-García, V. López-Puente, E.H. Hill, C. Hamon, M.N. Sanz-Ortiz, S. Rodal-Cedeira, C. Costas, S. Celiksoy, I. Pérez-Juste, L. Scarabelli, A. La Porta, J. Pérez-Juste, I. Pastoriza-Santos, L.M. Liz-Marzán, Detection and imaging of quorum sensing in Pseudomonas aeruginosa biofilm communities by surface-enhanced resonance Raman scattering, Nat. Mater. 15 (2016) 1203–1211, https://doi.org/10.1038/nmat4720.
[59] J. Zeng, Y. Zhang, T. Zeng, R. Aleisa, Z. Qiu, Y. Chen, J. Huang, D. Wang, Z. Yan, Y. Yin, Anisotropic plasmonic nanostructures for colorimetric sensing, Nano Today. 32 (2020), 100855, https://doi.org/10.1016/j.nantod.2020.100855.
[60] L. Wang, W. Ma, L. Xu, W. Chen, Y. Zhu, C. Xu, N.A. Kotov, Nanoparticle-based environmental sensors, Mater. Sci. Eng. R Reports. 70 (2010) 265–274, https://doi.org/10.1016/j.mser.2010.06.012.
[61] A. Sánchez-Iglesias, P. Aldeanueva-Potel, W. Ni, J. Pérez-Juste, I. Pastoriza-Santos, R.A. Alvarez-Puebla, B.N. Mbenkum, L.M. Liz-Marzán, Chemical seeded growth of Ag nanoparticle arrays and their application as reproducible SERS substrates, Nano Today. 5 (2010) 21–27, https://doi.org/10.1016/j.nantod.2010.01.002.
[62] K.A. Homan, M. Souza, R. Truby, G.P. Luke, C. Green, E. Vreeland, S. Emelianov, Silver nanoplate contrast agents for in vivo molecular photoacoustic imaging, ACS Nano. 6 (2012) 641–650, https://doi.org/10.1021/nn204100n.
[63] H. Chen, Z. Zhen, T. Todd, P.K. Chu, J. Xie, Nanoparticles for improving cancer diagnosis, Mater. Sci. Eng. R Reports. 74 (2013) 35–69, https://doi.org/10.1016/j.mser.2013.03.001.
[64] S.K. Bae, D.C. Choo, H.S. Kang, K.H. Yoo, T.W. Kim, Transparent ultra-thin silver electrodes formed via a maskless evaporation process for applications in flexible organic light-emitting devices, Nano Energy. 71 (2020), 104649, https://doi.org/10.1016/j.nanoen.2020.104649.
[65] G. Baffou, J. Polleux, H. Rigneault, S. Monneret, Super-Heating and Micro-Bubble Generation around Plasmonic Nanoparticles under cw Illumination, J. Phys. Chem. C. 118 (2014) 4890–4898, https://doi.org/10.1021/jp411519k.
[66] S. Yoo, J. Lee, J. Kim, J.M. Kim, M. Haddadnezhad, S. Lee, S. Choi, D. Park, J. M. Nam, S. Park, Silver Double Nanorings with Circular Hot Zone, J. Am. Chem. Soc. 142 (2020) 12341–12348, https://doi.org/10.1021/jacs.0c04419.
[67] T. Tan, S. Zhang, J. Wang, Y. Zheng, H. Lai, J. Liu, F. Qin, C. Wang, Resolving the stacking fault structure of silver nanoplates, Nanoscale. 13 (2021) 195–205, https://doi.org/10.1039/D0NR06912D.
[68] K. Qi, Y. Zhang, J. Li, C. Charmette, M. Ramonda, X. Cui, Y. Wang, Y. Zhang, H. Wu, W. Wang, X. Zhang, D. Voiry, Enhancing the CO2-to-CO Conversion from 2D Silver Nanoprisms via Superstructure Assembly, ACS Nano. 15 (2021) 7682–7693, https://doi.org/10.1021/acsnano.1c01281.
[69] B. Ajitha, Y.A.K. Reddy, M.J. Kim, H.-J. Jeon, C.W. Ahn, Superior catalytic activity of synthesized triangular silver nanoplates with optimized sizes and shapes, Catal, Sci. Technol. 6 (2016) 8289–8299, https://doi.org/10.1039/C6CY01948J.
[70] J.Y. Cheon, S.J. Kim, W.H. Park, Facile Interpretation of Catalytic Reaction between Organic Dye Pollutants and Silver Nanoparticles with Different Shapes, J. Nanomater. 2019 (2019) 1–8, https://doi.org/10.1155/2019/3257892.
[71] R. Mravljak, O. Bizjak, P. Krajnc, M. Paljevac, A. Podgornik, Non-invasive determination of ionizable ligand group density on high internal phase emulsion derived polymer, J. Chromatogr. A. 1652 (2021), 462077, https://doi.org/10.1016/j.chroma.2021.462077.
[72] G.S. Métraux, C.A. Mirkin, Rapid Thermal Synthesis of Silver Nanoprisms with Chemically Tailorable Thickness, Adv. Mater. 17 (2005) 412–415, https://doi.org/10.1002/adma.200401086.
[73] Q. Zhang, N. Li, J. Goebl, Z. Lu, Y. Yin, A Systematic Study of the Synthesis of Silver Nanoplates: Is Citrate a "Magic" Reagent? J. Am. Chem. Soc. 133 (2011) 18931–18939, https://doi.org/10.1021/ja2080345.
[74] Z. Tang, Q. Zhang, Y. Yin, C.E.A. Chang, Facet selectivity of ligands on silver nanoplates: Molecular mechanics study, J. Phys. Chem. C. 118 (2014) 21589–21598, https://doi.org/10.1021/jp503319s.
[75] H. Zhao, T. Yang, D. Liu, L. Yin, T. Yang, F. Yin, H. Deng, W. Zhang, X. Liu, A novel method to regulate the morphology of silver nanostructure by galvanic replacement reaction with boric acid, Appl. Nanosci. 10 (2020) 3279–3285, https://doi.org/10.1007/s13204-020-01339-5.

[76] J. Zeng, X. Xia, M. Rycenga, P. Henneghan, Q. Li, Y. Xia, Successive Deposition of Silver on Silver Nanoplates: Lateral versus Vertical Growth, Angew. Chemie Int. Ed. 50 (2011) 244–249, https://doi.org/10.1002/anie.201005549.
[77] B.H. Kim, J.H. Oh, S.H. Han, Y.J. Yun, J.S. Lee, Combinatorial polymer library approach for the synthesis of silver nanoplates, Chem. Mater. 24 (2012) 4424–4433, https://doi.org/10.1021/cm3028115.
[78] K.M. Koczkur, S. Mourdikoudis, L. Polavarapu, S.E. Skrabalak, Polyvinylpyrrolidone (PVP) in nanoparticle synthesis, Dalt. Trans. 44 (2015) 17883–17905, https://doi.org/10.1039/C5DT02964C.
[79] D. He, A.M. Jones, S. Garg, A.N. Pham, T.D. Waite, Silver nanoparticle-reactive oxygen species interactions: Application of a charging-discharging model, J. Phys. Chem. C. 115 (2011) 5461–5468, https://doi.org/10.1021/jp111275a.
[80] D. He, S. Garg, T.D. Waite, H_2O_2 -Mediated Oxidation of Zero-Valent Silver and Resultant Interactions among Silver Nanoparticles, Silver Ions, and Reactive Oxygen Species, Langmuir. 28 (2012) 10266–10275, https://doi.org/10.1021/la300929g.
[81] H. Yu, Q. Zhang, H. Liu, M. Dahl, J.B. Joo, N. Li, L. Wang, Y. Yin, Thermal synthesis of silver nanoplates revisited: A modified photochemical process, ACS Nano. 8 (2014) 10252–10261, https://doi.org/10.1021/nn503459q.
[82] R. Grzeschik, D. Schäfer, T. Holtum, S. Küpper, A. Hoffmann, S. Schlücker, On the Overlooked Critical Role of the pH Value on the Kinetics of the 4-Nitrophenol NaBH 4 -Reduction Catalyzed by Noble-Metal Nanoparticles (Pt, Pd, and Au) , J. Phys. Chem. C. 124 (2020) acs.jpcc.9b07114. 10.1021/acs.jpcc.9b07114.
[83] J. Strachan, C. Barnett, A.F. Masters, T. Maschmeyer, 4-Nitrophenol Reduction: Probing the Putative Mechanism of the Model Reaction, ACS Catal. 10 (2020) 5516–5521, https://doi.org/10.1021/acscatal.0c00725.
[84] M.R. Buchmeiser, Polymeric monolithic materials: Syntheses, properties, functionalization and applications, Polymer (Guildf). 48 (2007) 2187–2198, https://doi.org/10.1016/j.polymer.2007.02.045.
[85] R.E. Parker, N.S. Isaacs, Mechanisms Of Epoxide Reactions, Chem. Rev. 59 (1959) 737–799, https://doi.org/10.1021/cr50028a006.
[86] K. Loza, J. Diendorf, C. Sengstock, L. Ruiz-Gonzalez, J.M. Gonzalez-Calbet, M. Vallet-Regi, M. Köller, M. Epple, The dissolution and biological effects of silver nanoparticles in biological media, J. Mater. Chem. B. 2 (2014) 1634, https://doi.org/10.1039/c3tb21569e.
[87] T.M. Pabst, G. Carta, pH transitions in cation exchange chromatographic columns containing weak acid groups, J. Chromatogr. A. 1142 (2007) 19–31, https://doi.org/10.1016/j.chroma.2006.08.066.
[88] N. Lendero, J. Vidič, P. Brne, A. Podgornik, A. Štrancar, Simple method for determining the amount of ion-exchange groups on chromatographic supports, J. Chromatogr. A. 1065 (2005) 29–38, https://doi.org/10.1016/j.chroma.2004.10.072.
[89] T.E. Bankston, L. Dattolo, G. Carta, pH Transients in hydroxyapatite chromatography columns-Experimental evidence and phenomenological modeling, J. Chromatogr. A. 1217 (2010) 2123–2131, https://doi.org/10.1016/j.chroma.2010.02.004.
[90] F. Smrekar, M. Ciringer, A. Štrancar, A. Podgornik, Characterisation of methacrylate monoliths for bacteriophage purification, J. Chromatogr. A. 1218 (2011) 2438–2444, https://doi.org/10.1016/j.chroma.2010.12.083.
[91] C.L. Yaws, The Yaws handbook of physical properties for hydrocarbons and chemicals : physical properties for more than 54,000 organic and inorganic chemical compounds, coverage for C1 to C100 organics and Ac to Zr inorganics, 2nd ed., Elsevier, Gulf Professional Publishing, 2015.
[92] U. Černigoj, U. Martinuč, S. Cardoso, R. Sekirnik, N.L. Krajnc, A. Štrancar, Sample displacement chromatography of plasmid DNA isoforms, J. Chromatogr. A. 1414 (2015) 103–109, https://doi.org/10.1016/j.chroma.2015.08.035.
[93] Ion Exchange Chromatography Principles and Methods, Gelifesciences. (2016) 167. https://research.fredhutch.org/content/dam/stripe/hahn/methods/biochem/Ion_Exchange_Chromatography_Handbook.pdf.
[94] F. Hu, S.C. Abeyweera, J. Yu, D. Zhang, Y. Wang, Q. Yan, Y. Sun, Quantifying Electrocatalytic Reduction of CO_2 on Twin Boundaries, Chem. 6 (2020) 3007–3021, https://doi.org/10.1016/j.chempr.2020.07.026.
[95] C. Yuan, Y. Xu, L. Zhong, L. Zhang, C. Yang, B. Jiang, Y. Deng, B. Zeng, N. He, W. Luo, L. Dai, Heterogeneous silver–polyaniline nanocomposites with tunable morphology and controllable catalytic properties, Nanotechnology. 24 (2013), 185602, https://doi.org/10.1088/0957-4484/24/18/185602.
[96] L. Zhang, X. Liu, Y. Wang, S. Xing, Controllable silver embedding into polypyrrole, J. Alloys Compd. 709 (2017) 431–437, https://doi.org/10.1016/j.jallcom.2017.03.172.
[97] G. Liao, J. Chen, W. Zeng, C. Yu, C. Yi, Z. Xu, Facile Preparation of Uniform Nanocomposite Spheres with Loading Silver Nanoparticles on Polystyrene-methyl Acrylic Acid Spheres for Catalytic Reduction of 4-Nitrophenol, J. Phys. Chem. C. 120 (2016) 25935–25944, https://doi.org/10.1021/acs.jpcc.6b09356.
[98] S.M. Alshehri, T. Almuqati, N. Almuqati, E. Al-Farraj, N. Alhokbany, T. Ahamad, Chitosan based polymer matrix with silver nanoparticles decorated multiwalled carbon nanotubes for catalytic reduction of 4-nitrophenol, Carbohydr. Polym. 151 (2016) 135–143, https://doi.org/10.1016/j.carbpol.2016.05.018.
[99] Y. Xia, Z. Gao, X. Liao, S. Yan, J. Han, X. Wang, C. Pan, Y. Zhang, W. Zhai, One-step green synthesis of silver nanobelts assisted by sodium carboxymethylcellulose for catalytic reduction of 4-nitrophenol, CrystEngComm. 20 (2018) 2135–2143, https://doi.org/10.1039/C8CE00031J.
[100] M.R. Schure, R.S. Maier, D.M. Kroll, H. Ted Davis, Simulation of ordered packed beds in chromatography, J. Chromatogr. A. 1031 (2004) 79–86. 10.1016/j.chroma.2003.12.030.
[101] A. Podgornik, Characterization of a convection-based support microstructure through a flow resistance parameter, J. Sep. Sci. (2022) 1–13, https://doi.org/10.1002/jssc.202100955.
[102] J.G. Fourie, J.P. Du Plessis, Pressure drop modelling in cellular metallic foams, Chem. Eng. Sci. 57 (2002) 2781–2789, https://doi.org/10.1016/S0009-2509(02)00166-5.
[103] H. Liu, P. Zhong, K. Liu, L. Han, H. Zheng, Y. Yin, C. Gao, Synthesis of ultrathin platinum nanoplates for enhanced oxygen reduction activity, Chem. Sci. 9 (2018) 398–404, https://doi.org/10.1039/C7SC02997G.
[104] R. Das, R.K. Soni, Synthesis and surface-enhanced Raman scattering of indium nanotriangles and nanowires, RSC Adv. 7 (2017) 32255–32263, https://doi.org/10.1039/C7RA03317F.
[105] J.-W. Lee, J. Han, D.S. Lee, S. Bae, S.H. Lee, S.-K. Lee, B.J. Moon, C.-J. Choi, G. Wang, T.-W. Kim, 2D Single-Crystalline Copper Nanoplates as a Conductive Filler for Electronic Ink Applications, Small. 14 (2018) 1703312, https://doi.org/10.1002/smll.201703312.
[106] S.S. Shankar, A. Rai, B. Ankamwar, A. Singh, A. Ahmad, M. Sastry, Biological synthesis of triangular gold nanoprisms, Nat. Mater. 3 (2004) 482–488, https://doi.org/10.1038/nmat1152.
[107] Y. Zhai, J.S. DuChene, Y.-C. Wang, J. Qiu, A.C. Johnston-Peck, B. You, W. Guo, B. DiCiaccio, K. Qian, E.W. Zhao, F. Ooi, D. Hu, D. Su, E.A. Stach, Z. Zhu, W. D. Wei, Polyvinylpyrrolidone-induced anisotropic growth of gold nanoprisms in plasmon-driven synthesis, Nat. Mater. 15 (2016) 889–895, https://doi.org/10.1038/nmat4683.
[108] Y. Xiong, J.M. McLellan, J. Chen, Y. Yin, Z.-Y. Li, Y. Xia, Kinetically Controlled Synthesis of Triangular and Hexagonal Nanoplates of Palladium and Their SPR/SERS Properties, J. Am. Chem. Soc. 127 (2005) 17118–17127, https://doi.org/10.1021/ja056498s.
[109] L. Xu, D. Liu, D. Chen, H. Liu, J. Yang, Size and shape controlled synthesis of rhodium nanoparticles, Heliyon. 5 (2019) e01165.
[110] Z. Xu, Z. Wei, P. He, X. Duan, Z. Yang, Y. Zhou, D. Jia, Seed-mediated growth of ultra-thin triangular magnetite nanoplates, Chem. Commun. 53 (2017) 11052–11055, https://doi.org/10.1039/C7CC05723G.
[111] T. Luo, Q.-Q. Meng, C. Gao, X.-Y. Yu, Y. Jia, B. Sun, Z. Jin, Q.-X. Li, J.-H. Liu, X.-J. Huang, Sub-20 nm-Fe_3O_4 square and circular nanoplates: synthesis and facet-dependent magnetic and electrochemical properties, Chem. Commun. 50 (2014) 15952–15955, https://doi.org/10.1039/C4CC06064D.
[112] J. Chandradass, D.S. Bae, K.H. Kim, Synthesis of γ-Al_2O_3 Hexagonal Nanoplatelet by Combining Sol-Gel and Hydrothermal Process, Mater. Manuf. Process. 25 (2010) 919–922, https://doi.org/10.1080/10426911003720771.
[113] V. Jordan, U. Javornik, J. Plavec, A. Podgornik, A. Rečnik, Self-assembly of multilevel branched rutile-type TiO_2 structures via oriented lateral and twin attachment, Sci. Rep. 6 (2016) 24216, https://doi.org/10.1038/srep24216.